Nonlinear Modeling of the Flux Linkage in 2-D Plane for the Planar Switched Reluctance Motor

Guang-Zhong Cao[1], Nan Chen[1], Su-Dan Huang[1], Song-Song Xiao[1], and Jiangbiao He[2]

[1]Shenzhen Key Laboratory of Electromagnetic Control, Shenzhen University, Shenzhen 518060, China
[2]GE Global Research, Schenectady, NY 12309 USA

This paper proposes a nonlinear flux linkage model in 2-D plane for the planar switched reluctance motor (PSRM). The inputs of the proposed model are the 2-D positions and the current, and the output is the flux linkage. The proposed model is established via a cascade-forward backpropagation neural network (CFNN). The designed CFNN consists of four layers: one input layer, two hidden layers, and one output layer. The first hidden layer has 20 neurons with a tan-sigmoid transfer function, and the second hidden layer has 20 neurons with a log-sigmoid transfer function. The output layer is a pure linear layer. The sample set with 179 755 samples is obtained experimentally in a dSPACE-based PSRM system by applying the dc excitation method. The sample set is divided into three sets. 35% and 30% of the samples are randomly chosen as the training sample set and validation sample set, respectively, and the remaining samples are utilized as the test sample set to assess the generalization performance of the CFNN-based model. According to the results of the test sample set, the maximum relative error is 11.05% and the mean relative error is 0.42% when the current ranges from 1 to 9 A. The CFNN has the capability to build a multi-input nonlinear model. The CFNN-based model is capable of reflecting the variations of flux linkage in 2-D plane caused by manufacturing tolerances. The effectiveness of the CFNN-based model is finally verified.

Index Terms— **Cascade-forward backpropagation neural network (CFNN), flux linkage in 2-D plane, nonlinear modeling, planar switched reluctance motor (PSRM).**

I. Introduction

PLANAR switched reluctance motors (PSRMs) are attractive candidates in precision 2-D positioning devices for applications in microscale manufacturing and semiconductor lithography because they have a simple structure, low cost, low heat loss, high precision, and high reliability in addition to being eco-friendly [1]–[4]. Flux linkage is the base of electromagnetic model and control for SRMs. Therefore, accurate modeling of the flux linkage plays a key role in achieving precise motion control of SRMs. However, modeling the flux linkage accurately for SRMs is difficult because they have a highly nonlinear magnetic field, which results from their inherently double salient structure and switched excitation. Modeling the flux linkage of PSRMs is particularly difficult due to their planar structure, as the tolerances of the tooth width, pole pitch, and air-gap are greater for planar structures than that for rotary and linear structures.

Nonlinear modeling of the flux linkage has been a reoccurring issue for SRMs [5]–[8]. According to the literature on SRMs [6], [7], [9], only a model of the flux linkage versus a one-axis position in a pole pitch has been built. The model of a pole pitch applied to all the positions is not accurate because of manufacturing tolerances for practical motors. However, the model is suitable for rotary SRMs because the manufacturing tolerances of rotary SRMs are smaller than those of other motors due to their larger pole pitch and the lower number of pole pairs in the rotary structure. For PSRMs, the mover moves in a 2-D plane with a long stroke, and it is more difficult to reduce the manufacturing tolerances for PSRMs than it is for rotary and linear SRMs. Based on the above-mentioned description, a nonlinear model of the flux linkage in a 2-D plane is more appropriate for PSRMs. Such a model is an effective method for yielding precise motion for PSRMs.

The neural network is able to handle nonlinear modeling with multiple inputs. Various neural networks, such as the B-spline neural network [10], feed-forward backpropagation neural network [9], and radial basis function neural network [11], [12], have been utilized in flux linkage modeling. All of the aforementioned neural networks are feed-forward neural network (FFNN). Besides, cascade-forward backpropagation neural network (CFNN) is also used to establish models [13], [14]. The CFNN is similar to the FFNN, where both of them use the backpropagation algorithm to update weights. However, the number of weight connections of the CFNN is larger than that of the FFNN, because each neuron of the latter layers is related to all neurons of all former layers [15]. For the same number of layers and neurons, the CFNN has more weights than the FFNN, and thus, the CFNN can carry more information from the samples. To accurately build the model of the flux linkage of the PSRM in 2-D plane, a large number of samples are inevitable. Hence, for the nonlinear modeling with a large number of samples, the utilization of the CFNN is more suitable than that of the FFNN. Based on the above-mentioned analysis, the CFNN is employed to build the nonlinear flux linkage model of the PSRM in 2-D plane.

In this paper, a nonlinear model of the flux linkage of the PSRM in 2-D plane is proposed using the CFNN. The remainder of this paper is organized as follows. In Section II, the mechanical structure of the PSRM is introduced. In Section III, the structure of the CFNN and training of the

Manuscript received March 15, 2018; revised April 28, 2018; accepted May 28, 2018. Date of publication June 28, 2018; date of current version October 17, 2018. Corresponding author: S.-D. Huang (e-mail: hsdsudan@gmail.com).

Color versions of one or more of the figures in this paper are available online at http://ieeexplore.ieee.org.

Digital Object Identifier 10.1109/TMAG.2018.2844551

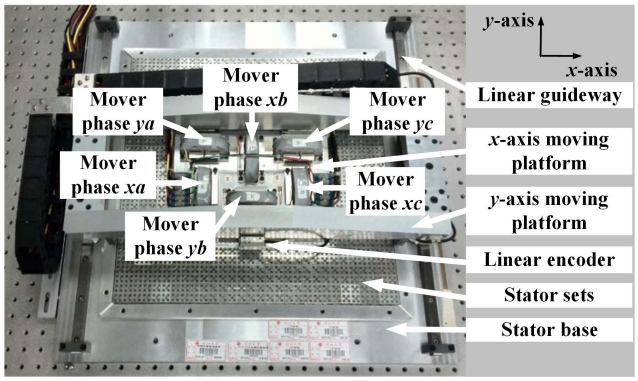

Fig. 1. Overall structure of the PSRM prototype.

CFNN are presented. In Section IV, the modeling results are given and discussed. Finally, Section V concludes this paper.

II. Mechanical Structure of the PSRM

The overall structure of the PSRM prototype developed in our laboratory [1]–[4] is shown in Fig. 1. The PSRM consists of x- and y-axis linear encoders, x- and y-axis linear guideways, x- and y-axis moving platforms, and stator sets and a stator base. The PSRM can be viewed as a combination of two orthometric linear SRMs. The six movers with two sets of three-phase windings are mounted on the x-axis moving platform. The pole pitch and range of the base plate of the PSRM are 7.2 mm and 600 mm × 600 mm, respectively.

III. Nonlinear Modeling of the Flux Linkage in 2-D Plane

A. Structure of the CFNN

The flux linkage in a phase of the PSRM can be represented as

$$\psi(p_x(t), p_y(t), i(t)) = i(t)L(p_x(t), p_y(t), i(t)) \tag{1}$$

where ψ is the flux linkage, p_x is the x-axis position, p_y is the y-axis position, i is the phase current, and L is the phase inductance. For a mover phase-lj (l is x- or y-axis; j is phases a, b, or c) of the PSRM, the phase inductance depends on the positions of the x- and y-axes in the 2-D plane and the phase current of the phase-lj; hence, the flux linkage also depends on the three variables. The inputs of the CFNN are the positions of the x- and y-axes and the phase-lj current. The flux linkage of phase-lj is the output of the CFNN.

Although a two-layer FFNN could potentially learn virtually any input–output relationship, a network with more layers and weight connections could learn complex relationships more precisely with a sufficiently large sample set. Thus, the designed CFNN has four layers, one input layer, two hidden layers, and one output layer; its structure is shown in Fig. 2. The first hidden layer has 20 neurons with a tan-sigmoid transfer function, and the second hidden layer has 20 neurons with a log-sigmoid transfer function. Tan-sigmoid and log-sigmoid are typical nonlinear transfer functions of neural network, which can represent the nonlinearity. To obtain better performance of nonlinear modeling, the combination of

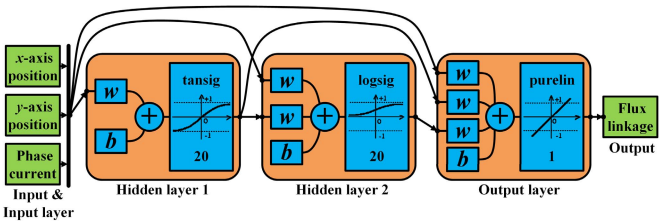

Fig. 2. Structure of the designed CFNN.

tan-sigmoid and log-sigmoid is applied. The output layer is linear, transferring all the outputs from all previous layers to a single output.

The time complexity of the designed CFNN is an important factor. In one forward calculation of the CFNN, the time complexity can be represented as

$$T = O\left[\sum_{m=1}^{\lambda-1}\left(\sum_{n=m+1}^{\lambda} s_m s_n\right)\right] = O(M) \tag{2}$$

where T is the time complexity, λ is the number of layers, s_m and s_n are the number of neurons in mth layer and nth layer, respectively, and M is the total number of weights in CFNN.

For the designed CFNN, λ is 4 and s of four layers is 3, 20, 20, and 1, respectively. Thus, M can be determined as 563. From (2), the time complexity is linear proportional to the total number of weights. In addition, the number of neurons with nonlinear transfer functions is 40, which is not large for neural network. Hence, the low time complexity is shown for the designed CFNN, and the computational complexity of the proposed model is not high.

B. Training of the CFNN

The experimentally obtained sample set is crucial for training and testing the CFNN and for the accuracy of the model. In this paper, the sample set used to train and test the CFNN is obtained from the mover phase-xb using a dc excitation method [16], which is capable of providing a large number of samples.

The experimental devices used to obtain samples are shown in Fig. 3. Acquisition of samples involves fixing the PSRM movers in different positions on the 2-D plane, injecting a dc excitation signal to the phase winding, and sampling the current and voltage in the phase-xb simultaneously. The sample acquisition uses the dSPACE-based PSRM system with a sampling frequency of 10 kHz. The flux linkage in phase-xb can be simultaneously calculated in the system according to

$$\psi(p_x(t), p_y(t), i(t))\big|_{p_x, p_y=\text{const}} = \int_0^t (u(\tau) - Ri(\tau))d\tau \tag{3}$$

where u is the phase voltage and R is the resistance of phase winding. The current rises from 0 to 9 A in each excitation process in less than 50 ms; therefore, the temperature rise of phase resistance can be ignored. The phase-xb resistance R is deemed a constant at the measured value of 0.473 Ω. In a fixed position with an x of 7.2 mm and y of 10.8 mm, the sampled phase voltage and phase current are shown in Fig. 4(a), and the calculated flux linkage is shown in Fig. 4(b).

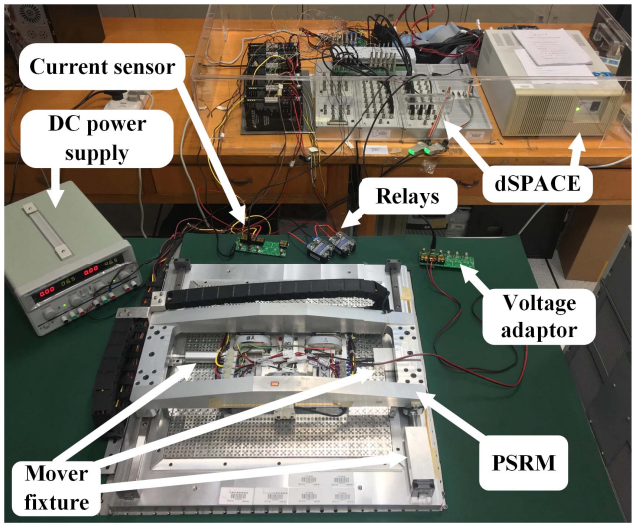

Fig. 3. Experimental devices for sample acquisition.

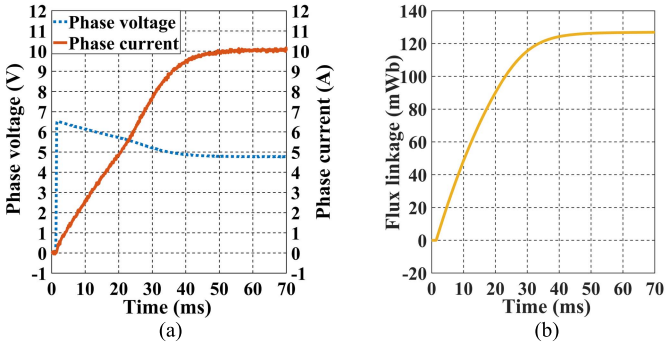

Fig. 4. Samples obtained from the dSPACE-based PSRM system. (a) Waveform of the sampled phase voltage and phase current. (b) Waveform of the calculated flux linkage.

The sample set of the phase-*xb* flux linkage versus the x-axis position versus the y-axis position versus the phase-*xb* current is obtained via the experimental measurements. In this sample set, the x-axis position ranges from 0 to 14.4 mm with interval of 0.4 mm; the y-axis position ranges from 0 to 21.6 mm with interval of 1.8 mm; the current ranges from 0 to 9 A. The sample set contains 179 755 samples and all of those are divided randomly to three sample sets. 35% of the samples are the training sample set to train the CFNN-based model, and 30% of the samples are the validation sample set to prevent the problem of overfitting in training process. The remaining samples are used as the test sample set to assess the generalization performance of the CFNN-based model.

The designed CFNN is trained for 1212 epochs using the Levenberg–Marquardt algorithm. The network error function is represented as

$$E(\boldsymbol{w}) = \frac{1}{2}\sum_{i=1}^{N}(y_i - \tilde{y}_i)^2 = \frac{1}{2}\sum_{i=1}^{N} e_i^2(\boldsymbol{w}) = \frac{1}{2}\boldsymbol{e}(\boldsymbol{w})^T\boldsymbol{e}(\boldsymbol{w}) \quad (4)$$

$$\boldsymbol{e}(\boldsymbol{w}) = [e_1(\boldsymbol{w}), e_2(\boldsymbol{w}), \ldots, e_N(\boldsymbol{w})]^T \quad (5)$$

where $\boldsymbol{w}$ is the weight vector, $e_i = y_i - \tilde{y}_i$, y_i and $\tilde{y}_i$ represent the sample of actual flux linkage and CFNN output, respectively, and N is the dimension of the output vector.

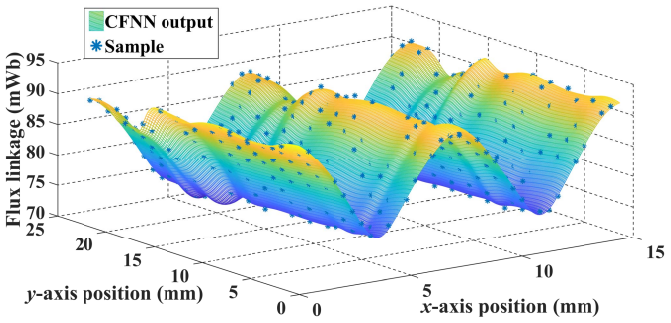

Fig. 5. For phase current of 5 A, the flux linkage from the CFNN-based model and the actual flux linkage from all samples.

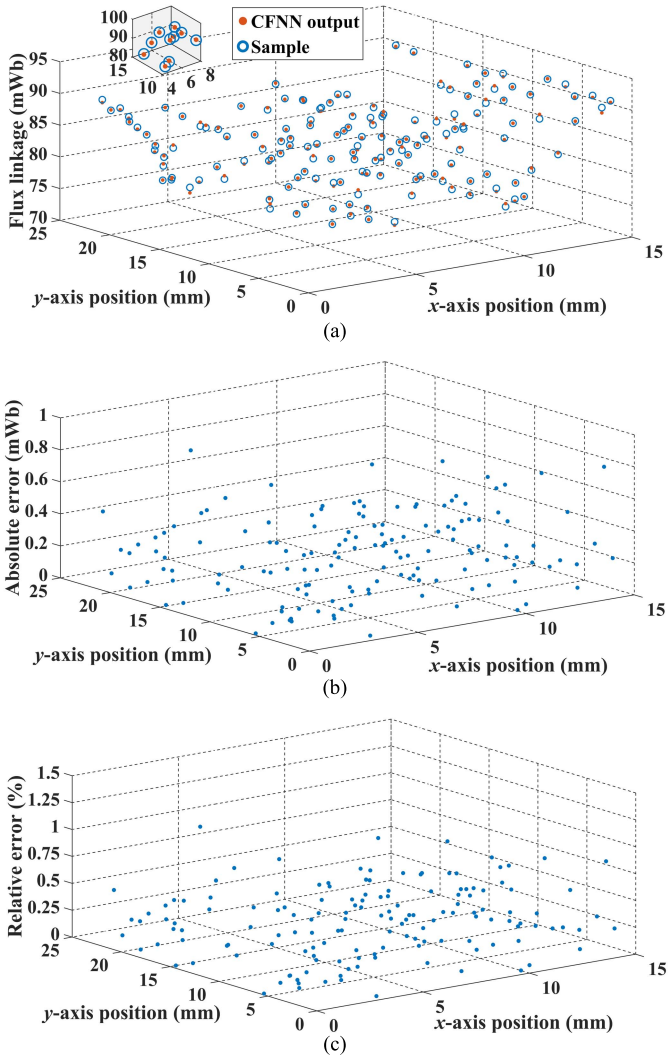

Fig. 6. Test results of the generalization performance of CFNN-based flux linkage versus x-axis position versus y-axis position at a phase current of 5 A. (a) CFNN-based and actual flux linkage. (b) Absolute error. (c) Relative error.

Update of the $\boldsymbol{w}$ at the kth step is represented as

$$\begin{aligned}\boldsymbol{w}_{k+1} &= \boldsymbol{w}_k + \Delta\boldsymbol{w}_k \\ &= \boldsymbol{w}_k - [\boldsymbol{J}(\boldsymbol{w}_k)^T\boldsymbol{J}(\boldsymbol{w}_k) + \mu\boldsymbol{I}]^{-1}\boldsymbol{J}(\boldsymbol{w}_k)^T\boldsymbol{e}(\boldsymbol{w}_k)\end{aligned} \quad (6)$$

where $\boldsymbol{J}(\boldsymbol{w}_k)$ is the Jacobian matrix, $\boldsymbol{J}(\boldsymbol{w}_k) = \partial\boldsymbol{e}(\boldsymbol{w}_k)/\partial\boldsymbol{w}_k$, μ is a positive damping term, and I is the identity matrix.

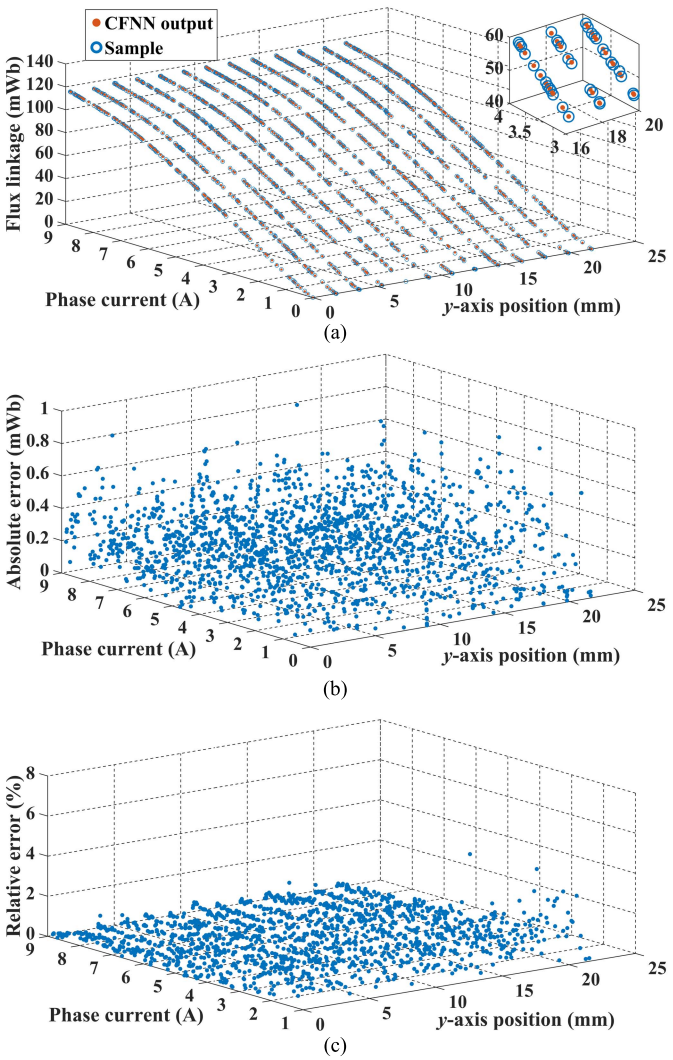

Fig. 7. Test results of the generalization performance of CFNN-based flux linkage versus y-axis position versus phase current at an x-axis position of 3.6 mm. (a) CFNN-based and actual flux linkage. (b) Absolute error. (c) Relative error with a phase current range of 1–9 A.

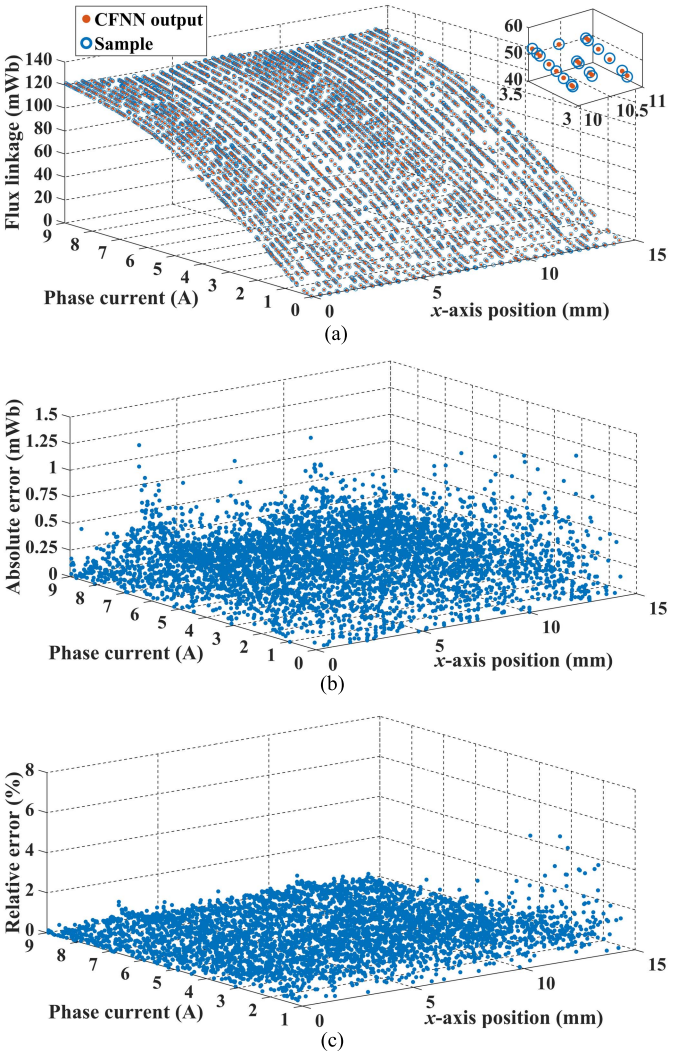

Fig. 8. Test results of the generalization performance of CFNN-based flux linkage versus x-axis position versus phase current at a y-axis position of 16.2 mm. (a) CFNN-based and actual flux linkage. (b) Absolute error. (c) Relative error with a phase current range of 1–9 A.

IV. Results and Discussion

For phase current of 5 A, the flux linkage from the CFNN-based model and the actual flux linkage from all samples are presented in Fig. 5. The generalization performance of the CFNN-based flux linkage model is assessed through the test sample set, and results are illustrated in Figs. 6–8.

From Fig. 5, at the same phase current of 5 A, the sampled phase-xb flux linkage is clearly related to the x-axis position, but is simultaneously affected by the y-axis position. Furthermore, at the same phase current, the same y-axis position, and the different x-axis position with the same relative position between the mover and stator, the phase-xb flux linkage is not identical. The above-mentioned issues, which mainly result from the manufacturing tolerances, are modeled in the CFNN-based flux linkage model.

The errors between the output of the CFNN-based model and the actual flux linkage are listed in Table I. The maximum absolute errors during the training and test are 1.534 and 1.644 mWb, respectively. The mean absolute errors during the training and test are 0.230 and 0.233 mWb, respectively. When current is less than 1 A, the maximum relative errors and mean relative errors are 55.90% and 7.17% in training and 53.87% and 7.34% in testing, respectively. At other current values, the maximum relative errors and mean relative errors are 7.81% and 0.42% in training and 11.05% and 0.42% in testing, respectively.

For currents less than 1 A, the relative errors are larger when the flux linkage is close to zero. In this condition, small absolute errors may produce large relative errors. However, the operating phase currents of the PSRM are greater than 1 A generally. When the phase current ranges from 1 to 9 A, for the three sample sets, the absolute error is less than 1.644 mWb, and the mean relative error is less than 0.43%. Hence, the generalization performance and effectiveness of the proposed nonlinear flux linkage model for the PSRM are verified.

TABLE I
ERRORS BETWEEN THE CFNN-BASED MODEL OUTPUT AND ACTUAL FLUX LINKAGE

	Maximum absolute error	Mean absolute error	Maximum relative error		Mean relative error	
	i of [0, 9] A	i of [0, 9] A	i of (0, 1) A	i of [1, 9] A	i of (0, 1) A	i of [1, 9] A
Training sample set	1.534 mWb	0.230 mWb	55.90%	7.81%	7.17%	0.42%
Validation sample set	1.613 mWb	0.232 mWb	58.05%	10.75%	7.55%	0.43%
Test sample set	1.644 mWb	0.233 mWb	53.87%	11.05%	7.34%	0.42%

V. CONCLUSION

In this paper, a nonlinear flux linkage model in a 2-D plane was proposed based on a CFNN with a sample set obtained experimentally from the dSPACE-based PSRM system. With the small current range of 0–1 A for the test sample set, the maximum relative error of 53.87% and the mean relative error of 7.34% are rather large, because the actual flux linkage is close to zero. For currents greater than 1 A, the maximum and mean relative errors decrease rapidly to 11.05% and 0.42%, respectively. The results demonstrate the generalization performance and effectiveness of the proposed CFNN-based model. Furthermore, the variations of the flux linkage in 2-D plane caused by manufacturing tolerances are reflected in the CFNN-based model as well. Therefore, the proposed nonlinear modeling of the flux linkage in 2-D plane is appropriate for precision positioning applications of PSRMs.

ACKNOWLEDGMENT

This work was supported in part by the National Natural Science Foundation of China under Grant 51677120 and Grant 51275312, in part by the Natural Science Foundation of Guangdong Province, China under Grant 2017A030310460, in part by the Shenzhen Government Fund under Grant KJYY20160428170944786 and Grant JCYJ20160520175515548, and in part by the Fundamental Research Funds for the Shenzhen University under Grant 2017039.

REFERENCES

[1] S.-D. Huang *et al.*, "Maximum-force-per-ampere strategy of current distribution for efficiency improvement in planar switched reluctance motors," *IEEE Trans. Ind. Electron.*, vol. 63, no. 3, pp. 1665–1675, Mar. 2016.

[2] S. D. Huang, G. Z. Cao, Z. Y. He, J. F. Pan, J. A. Duan, and Q. Q. Qian, "Nonlinear modeling of the inverse force function for the planar switched reluctance motor using sparse least squares support vector machines," *IEEE Trans. Ind. Informat.*, vol. 11, no. 3, pp. 591–600, Jun. 2015.

[3] G.-Z. Cao, L.-L. Li, S.-D. Huang, L.-M. Li, Q.-Q. Qian, and J.-A. Duan, "Nonlinear modeling of electromagnetic forces for the planar-switched reluctance motor," *IEEE Trans. Magn.*, vol. 51, no. 11, Nov. 2015, Art. no. 8206605.

[4] G.-Z. Cao, J.-L. Fang, S.-D. Huang, J.-A. Duan, and J. F. Pan, "Optimization design of the planar switched reluctance motor on electromagnetic force ripple minimization," *IEEE Trans. Magn.*, vol. 50, no. 11, Nov. 2014, Art. no. 8203404.

[5] J. Du, D. Liang, and X. Liu, "Performance analysis of a mutually coupled linear switched reluctance machine for direct-drive wave energy conversions," *IEEE Trans. Magn.*, vol. 53, no. 9, Sep. 2017, Art. no. 8108110.

[6] R. Zhong *et al.*, "Accurate model of switched reluctance motor based on indirect measurement method and least square support vector machine," *IET Electr. Power Appl.*, vol. 10, no. 9, pp. 916–922, Nov. 2016.

[7] H. Chen, W. Yan, and Q. Wang, "Electromagnetic analysis of flux characteristics of double-sided switched reluctance linear machine," *IEEE Trans. Appl. Supercond.*, vol. 26, no. 4, p. 7, Jun. 2016, Art. no. 0603407.

[8] O. Ustun, "Measurement and real-time modeling of inductance and flux linkage in switched reluctance motors," *IEEE Trans. Magn.*, vol. 45, no. 12, pp. 5376–5382, Dec. 2009.

[9] S. Song, L. Ge, and M. Zhang, "Data-reconstruction-based modeling of SRM with few flux-linkage samples from torque-balanced measurement," *IEEE Trans. Energy Convers.*, vol. 31, no. 2, pp. 424–435, Jun. 2016.

[10] Z. Lin, D. S. Reay, B. W. Williams, and X. He, "Online modeling for switched reluctance motors using B-spline neural networks," *IEEE Trans. Ind. Electron.*, vol. 54, no. 6, pp. 3317–3322, Dec. 2007.

[11] L. Ortombina, F. Tinazzi, and M. Zigliotto, "Magnetic modeling of synchronous reluctance and internal permanent magnet motors using radial basis function networks," *IEEE Trans. Ind. Electron.*, vol. 65, no. 2, pp. 1140–1148, Feb. 2018.

[12] J. Cai, Z. Q. Deng, R. Y. Qi, Z. Y. Liu, and Y. H. Cai, "A novel BVC-RBF neural network based system simulation model for switched reluctance motor," *IEEE Trans. Magn.*, vol. 47, no. 4, pp. 830–838, Apr. 2011.

[13] S. Tengeleng and N. Armand, "Performance of using cascade forward back propagation neural networks for estimating rain parameters with rain drop size distribution," *Atmosphere*, vol. 5, no. 2, pp. 454–472, 2014.

[14] M. Lashkarbolooki, Z. S. Shafipour, and A. Z. Hezave, "Trainable cascade-forward back-propagation network modeling of spearmint oil extraction in a packed bed using SC-CO_2," *J. Supercritical Fluids*, vol. 73, pp. 108–115, Jan. 2013.

[15] A. M. Ameen, J. Pasupuleti, T. Khatib, W. Elmenreich, and H. A. Kazem, "Modeling and characterization of a photovoltaic array based on actual performance using cascade-forward back propagation artificial neural network," *J. Sol. Energy Eng.*, vol. 137, no. 4, p. 041010, 2015.

[16] H. X. Zheng, G. Z. Cao, S. D. Huang, L. L. Li, and L. M. Li, "A thrust force characteristics measurement of the planar switched reluctance motor using flux linkage characteristics," in *Proc. 17th Int. Conf. Elect. Mach. Syst. (ICEMS)*, Oct. 2014, pp. 2859–2862.